Table A.4. The derived distance-*FWHM* relation and *FWHM* at 2 kpc for the different simulations.

SNR	Contains clumps?	Contains large-scale structure?	Fit 1 slope [$\times 10^{-4}$ pc]	Fit 1 intercept [pc]	Fit 1 ΔF [pc]	Fit 2 slope [$\times 10^{-4}$ pc]	Fit 2 intercept [pc]	Fit 2 ΔF [pc]
100	✓	✓	1.67±0.13	0.10	4.3±0.3	1.11±0.13	0.25±0.02	4.8±0.3
10	✓	✓	1.64±0.10	0.10	4.3±0.2	1.14±0.09	0.24±0.02	4.7±0.2
100	-	✓	1.85±0.13	0.10	4.7±0.3	1.18±0.13	0.29±0.02	5.2±0.3
10	-	✓	1.80±0.15	0.10	4.6±0.3	1.15±0.17	0.28±0.02	5.1±0.3
100	-	-	1.03±0.04	0.10	3.1±0.1	0.93±0.05	0.13±0.00	3.1±0.1
10	-	-	1.02±0.05	0.10	3.0±0.1	0.91±0.06	0.13±0.01	3.1±0.1
100	✓	-	0.97±0.04	0.10	2.9±0.1	0.90±0.04	0.12±0.01	3.0±0.1
10	✓	-	0.97±0.06	0.10	2.9±0.1	0.90±0.06	0.12±0.01	3.0±0.1

Notes. Fit 1 assumes an intrinsic 0.1 pc width, Fit 2 leaves the intrinsic width as a free parameter. Values are the mean ± standard deviation of a sample of 20 random realizations. Increase in *FWHM* is defined as $\Delta F = FWHM_{(d=2\,\mathrm{kpc})}\ /\ FWHM_{\mathrm{True}}$, where $FWHM_{\mathrm{True}} = 0.1$ pc.

tion. We thus perform tests of a simulated filament with *SNR* = 100 and convolution kernel $\sigma = 3.0$, and fit symmetric Plummer models both with 1-D and 2-D convolution.

We perform this test with three filaments of varying background fluctuation, shown in Fig. A.7, frames d, h, and l. The median profiles for the original filament components are shown in the first column, the 1-D fit in the second in purple, and the 2-D fit in the third in gray. Derived Plummer parameters are listed in Table A.5. Violin plots of derived R_{flat}, p, and *FWHM* are shown in Fig. A.8.

As seen in the previous section, increasing filament strength results in decreased spread in Plummer parameters. The spread in 1-D convolution is larger, as adjacent rows are not so well correlated. In fields with $SNR_{\mathrm{filament}} > 8$, the median values are very similar. This is especially true for *FWHM*, in which the median values differ by under 10%. Due to its faster computing time (Fig. A.9), the 1-D convolution is a viable choice.

Appendix B: Additional tables

We present additional tables and data used in this paper. Fig. B.1 shows the three other ArTéMiS fields. Centers of the empty reference regions are listed in Table B.2, uncertainties on symmetric and asymmetric fits to an ideal filament in Tables B.3 and B.4, and median SNR_{filament} of each field in Table B.5 for all quality flags. Finally, the results of wavelet analysis are shown in Table B.6.

Appendix C: Testing the flux recovery of uvcombine

To test whether feathering recovered all flux, we performed simulations of an ideal filament with several Gaussian clumps. A Plummer filament and the clumps are shown in Fig. C.1a. The ideal map was convolved with a beam of 25″ and white noise amounting to 1% of peak emission added to create the *Herschel* image (Fig. C.1b). The small-scale ArTéMiS image (Fig. C.1c) was created by subtracting an image convolved by 2′ from an image convolved by 8.5″, then adding white noise of 2% of peak emission.

The feathered result is shown in frame d, and the difference between the ideal and feathered images in frame e. The difference is under three percent of the original flux, showing that most signal is recovered by feathering. This effect worsens with decreasing SNR, but is not significant especially in q = 1–2 filaments.

Appendix D: Plummer parameters

The following section presents derived Plummer parameters for the three regions studied in this paper. Tables D.1-D.2 list median derived Plummer parameters for asymmetric and symmetric fits. Violin plots of the same results are shown in Fig. D.1 for asymmetric fits.

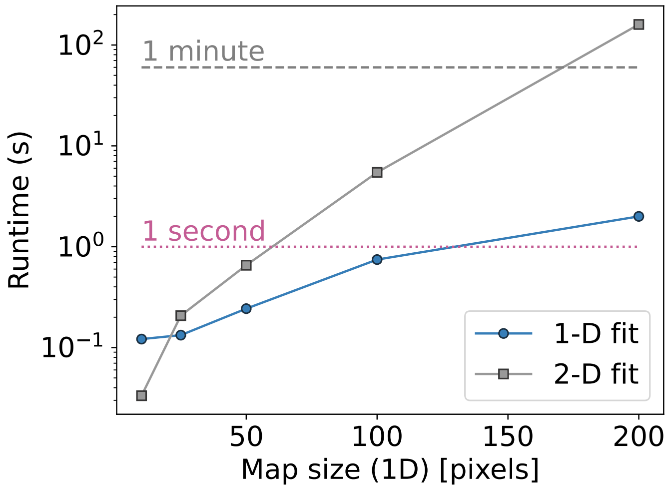

Fig. A.9. Time taken to run 1-D (blue circles) and 2-D (gray squares) Plummer analysis of maps of various sizes. These maps have a high SNR, comparable to the third row in Fig. A.7.

Table B.1. Parameters of the ArTéMiS observations

Field	RMS noise ($\mathrm{MJy\,sr^{-1}}$)	Max. signal ($\mathrm{MJy\,sr^{-1}}$)	Max. SNR
G16	254.6	1174.7	4.6
G17	133.5	612.7	4.6
G202	140.0	1970.6	14.1
G208	181.7	12452.0	68.5

Table B.2. Coordinates and radii of the reference regions used for noise estimation.

Field	ra (°)	dec (°)	radius (°)	instrument
G017.69-00.15	275.26	-13.92	0.03	*Herschel*
G202.16+02.64	100.39	10.65	0.03	*Herschel*
G208.63-20.36	83.69	-5.00	0.03	*Herschel*
G16	275.16	-14.07	0.02	ArTéMiS
G17	273.53	-12.73	0.02	ArTéMiS
G202	100.22	10.59	0.02	ArTéMiS
G208	83.89	-5.04	0.02	ArTéMiS

Table B.3. Uncertainties on symmetric fits of a simulated filament.

(1) Variable	(2) Initial value	(3) Mean ± std	(4) Median
R_{flat} (pix)	6.0	5.9 ± 0.25	5.9
p	1.75	1.73 ± 0.044	1.72
$FWHM$ (pix)	27.8	28.3 ± 0.83	28.2
Δr (10^{-2} pix)	0.0	-0.36 ± 2.0	-0.41
a	0.00	-0.00 ± 0.020	-0.00
b (10^{-3})	0.2	0.2 ± 0.02	0.2
N_0 ($10^{22}\,\mathrm{cm^{-2}}$)	1.0	1.0 ± 0.02	1.0

Notes. Plummer parameters of a simulated filament over a powerlaw background. The initial Plummer parameters are listed in column 2, the mean ± standard deviation recovered values in column 3, and the median recovered value in column 4.

Table B.4. Uncertainties on asymmetric fits of a simulated filament.

(1) Variable	(2) Initial value	(3) Mean ± std	(4) Median
R_{L} (pix)	6.0	6.0± 0.40	6.1
R_{R} (pix)	6.0	5.9 ± 0.41	5.9
$\langle R_{\mathrm{flat}} \rangle$ (pix)	6.0	5.9± 0.24	6.0
p_1	1.75	1.75± 0.054	1.75
p_2	1.75	1.73± 0.061	1.73
$\langle p \rangle$	1.75	1.74± 0.048	1.74
$FWHM$ (pix)	27.8	27.9± 1.01	27.8
Δr (pix)	0.0	-0.023± 0.19	-0.047
a	0.00	0.00± 0.023	0.00
b (10^{-3})	0.2	0.1± 0.2	0.1
N_0 ($10^{22}\,\mathrm{cm^{-2}}$)	1.0	1.0 ± 0.03	1.0

Notes. Same as Table B.3, but using an asymmetric Plummer fit.

Table B.5. Median SNR of the filament in each quality flag.

Field	SNR			
	$q = 1$	2	3	4
G17	12.6	9.1	6.9	4.5
G202	63.8	39.7	28.8	22.1
G208 $N_{\mathcal{H}}$	31.1	14.6	8.5	4.4
G208 $N_{\mathcal{H},\mathrm{crop}}$	122.6	67.2	51.1	28.4
G208 $N_{\mathcal{F}}$	100.9	54.1	39.4	21.0

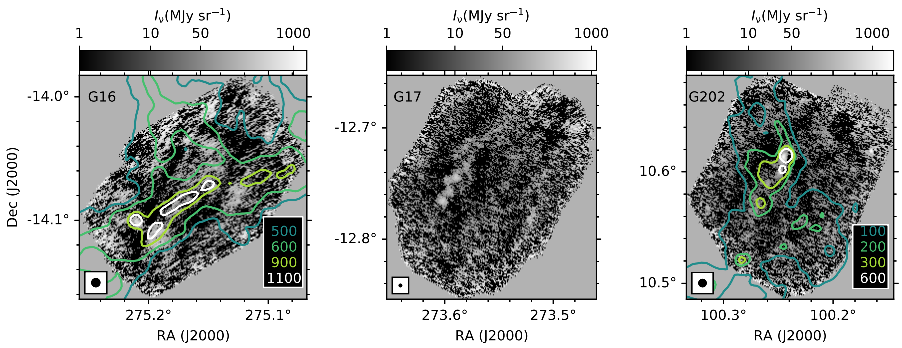

Fig. B.1. ArTéMiS 350 μm surface brightness maps (grayscale) of the G16, G17, and G202 fields. For G16 and G202, the contours show *Herschel* 350 μm surface brightness, with contour levels (in MJy/sr) listed in the frames. The *Herschel* beam is shown in the G16 and G202 frames, and the ArTéMiS beam in the G17 frame.

Table B.6. Results of the wavelet analysis in Sect. 3.6.2.

Field	Level	Size (pc)	$n_{\rm struct}$	$\langle N(H_2)\rangle$ ($\times10^{22}$ cm^{-2})	$\langle n(H)\rangle$ (10^5 cm^{-3})	$\sum M$ ($M_\odot$)	$\langle s\rangle$ (pc)
G017	10	3.0	2	1.01	0.06	2192.4	6.32
	9	2.0	3	1.46	0.17	1062.0	3.04
	8	1.0	4	1.70	0.28	936.8	1.79
	7	0.75	5	1.77	0.39	618.9	-
	6	0.5	8	1.84	0.55	449.5	-
	5	0.25	10	1.81	0.68	357.5	0.81
	4	0.1	9	1.82	0.75	293.2	-
	3	0.075	9	1.82	0.74	289.4	-
G202	8	1.0	1	0.70	0.00	409.5	1.82
	7	0.75	1	0.72	0.00	399.8	0.89
	6	0.5	3	0.80	0.15	226.7	-
	5	0.25	5	1.06	0.31	149.2	0.33
	4	0.1	3	1.58	0.55	147.7	-
	3	0.075	7	1.54	0.94	60.8	-
	2	0.05	9	1.52	1.14	63.0	-
	1	0.025	9	1.53	1.16	63.0	0.30
G208 ($N_{\mathcal{H}}$)	8	1.0	1	2.53	0.00	607.2	1.07
	7	0.75	1	2.37	0.00	641.4	-
	6	0.5	2	3.27	0.68	431.7	0.55
	5	0.25	1	2.63	0.00	110.6	0.32
	4	0.1	4	5.14	2.37	121.8	0.20
	3	0.075	4	11.03	8.69	162.1	-
	2	0.05	7	13.66	19.38	50.7	0.11
	1	0.025	7	13.52	19.85	48.5	-
G208 ($N_{\mathcal{F}}$)	6	0.5	1	2.88	0.00	162.9	-
	5	0.25	1	3.75	0.00	134.5	0.35
	4	0.1	0	-	-	0.0	0.14
	3	0.075	3	5.43	5.68	52.5	-
	2	0.05	5	6.57	14.14	22.8	0.09
	1	0.025	9	6.33	15.83	28.6	0.03

Notes. Columns 2-3 list the sizes of the structures in each category, column 4 the number of structures, columns 5-6 the mean column and volume densities, column 7 the total gas mass, and column 8 the separation between adjacent structures.

Table D.1. Median asymmetric Plummer parameters for our data.

Field	Qual	N_0 (10^{22} cm^{-2})	$R_{\text{flat,L}}$ (pc)	p_{L}	$R_{\text{flat,R}}$ (pc)	p_{R}	Δr (pc)	a (10^{22} cm^{-2})	b (10^{22} cm^{-2} pc^{-1})	*FWHM* (pc)
G017	1	1.80 ± 0.37	0.32 ± 1.51	2.24 ± 2.77	0.50 ± 0.42	3.71 ± 2.61	-0.35 ± 0.63	-0.00 ± 0.11	0.00 ± 0.03	0.89 ± 0.75
	1-2	1.58 ± 0.48	0.32 ± 1.77	2.40 ± 3.42	0.50 ± 1.46	3.62 ± 2.58	-0.36 ± 1.04	-0.00 ± 0.13	-0.00 ± 0.03	0.95 ± 1.94
	1-3	1.34 ± 0.51	0.44 ± 1.68	3.11 ± 3.19	0.41 ± 1.46	2.88 ± 2.51	-0.19 ± 1.02	-0.00 ± 0.11	-0.00 ± 0.03	0.99 ± 1.87
	1-4	1.29 ± 0.55	0.43 ± 1.71	2.95 ± 3.24	0.42 ± 1.39	2.87 ± 2.42	-0.13 ± 0.98	-0.00 ± 0.11	-0.00 ± 0.03	1.06 ± 1.79
G202	1	1.35 ± 0.09	0.08 ± 0.04	2.34 ± 0.49	0.10 ± 0.08	1.92 ± 1.23	0.02 ± 0.05	0.02 ± 0.03	0.01 ± 0.04	0.28 ± 0.04
	1-2	0.94 ± 0.22	0.20 ± 0.90	2.95 ± 2.97	0.08 ± 0.50	2.13 ± 1.93	-0.05 ± 0.46	0.00 ± 0.02	0.00 ± 0.03	0.49 ± 0.45
	1-3	0.84 ± 0.27	0.23 ± 0.80	2.97 ± 3.57	0.09 ± 0.79	2.18 ± 3.29	0.02 ± 0.49	-0.00 ± 0.02	0.00 ± 0.03	0.61 ± 0.45
	1-4	0.68 ± 0.29	0.30 ± 0.76	3.17 ± 3.82	0.12 ± 0.74	2.17 ± 2.87	0.03 ± 0.45	-0.00 ± 0.02	0.00 ± 0.03	0.78 ± 0.50
G208 $N_{\mathcal{H}}$	1	11.90 ± 6.94	0.07 ± 0.11	4.18 ± 3.87	0.06 ± 0.04	2.79 ± 0.80	0.02 ± 0.03	-0.00 ± 0.06	-0.02 ± 0.06	0.11 ± 0.03
	1-2	6.26 ± 6.34	0.06 ± 0.07	2.75 ± 2.80	0.07 ± 0.05	2.99 ± 1.47	0.02 ± 0.02	-0.00 ± 0.04	0.01 ± 0.07	0.14 ± 0.03
	1-3	5.17 ± 5.84	0.06 ± 0.22	2.75 ± 3.17	0.07 ± 0.06	3.01 ± 1.62	0.01 ± 0.03	-0.00 ± 0.03	0.01 ± 0.10	0.14 ± 0.09
	1-4	3.58 ± 5.49	0.07 ± 0.20	3.08 ± 3.05	0.07 ± 0.17	2.99 ± 1.77	0.02 ± 0.05	-0.00 ± 0.03	0.01 ± 0.09	0.15 ± 0.11
G208 $N_{\mathcal{H},\text{crop}}$	1	8.15 ± 0.09	0.10 ± 0.01	9.23 ± 1.79	0.05 ± 0.00	4.58 ± 0.79	0.00 ± 0.01	1.29 ± 0.05	1.89 ± 0.85	0.08 ± 0.00
	1-2	5.00 ± 1.80	0.06 ± 0.02	5.19 ± 2.56	0.06 ± 0.04	5.01 ± 2.85	0.00 ± 0.01	0.75 ± 0.42	1.21 ± 0.71	0.08 ± 0.02
	1-3	4.05 ± 1.91	0.07 ± 0.03	5.28 ± 3.27	0.05 ± 0.12	4.36 ± 3.08	0.00 ± 0.01	0.49 ± 0.40	0.90 ± 2.44	0.08 ± 0.14
	1-4	3.14 ± 2.11	0.11 ± 0.05	6.95 ± 3.96	0.05 ± 0.12	3.10 ± 2.66	-0.00 ± 0.01	0.26 ± 0.39	0.49 ± 1.94	0.10 ± 0.11
G208 $N_{\mathcal{F}}$	1	12.96 ± 4.31	0.04 ± 0.03	3.67 ± 2.47	0.02 ± 0.02	2.07 ± 0.86	0.00 ± 0.01	-0.00 ± 0.68	0.00 ± 4.82	0.05 ± 0.02
	1-2	10.36 ± 4.85	0.03 ± 0.03	2.88 ± 2.84	0.02 ± 0.03	2.09 ± 1.82	0.01 ± 0.01	-0.00 ± 0.58	1.19 ± 4.92	0.05 ± 0.02
	1-3	6.89 ± 4.90	0.04 ± 0.03	3.10 ± 2.61	0.02 ± 0.04	2.05 ± 2.74	0.00 ± 0.02	-0.00 ± 0.50	0.70 ± 4.85	0.06 ± 0.02
	1-4	6.12 ± 5.09	0.04 ± 0.04	3.10 ± 2.81	0.02 ± 0.04	2.02 ± 2.59	0.00 ± 0.02	-0.00 ± 0.47	0.70 ± 4.51	0.07 ± 0.03

Notes. Median Plummer parameters for asymmetric Plummer fits to *Herschel* SPIRE+PACS 160 μm column density data (Image *FWHM* = 20″) and the $N_{\mathcal{F}}$ data, only including those fits for which $\langle p_{\text{R}}, p_{\text{L}} \rangle \leq 10$. Errors are the 1-$\sigma$ standard deviation. Note these are calculated using the median of all derived Plummer parameters, *not* the fit to the median filament profile. R_{L} and p_{L} refer to fits to the left-hand side of the filament, R_{R} and p_{R} to the right-hand side.

Table D.2. Median symmetric Plummer parameters for our data.

Field	Qual	N_0 (10^{22} cm^{-2})	$R_{\rm flat}$ (pc)	p	a (10^{22} cm^{-2})	b (10^{22} cm^{-2} pc^{-1})	Δr (pc)	$FWHM$ (pc)
G017	1	1.87 ± 0.40	0.43 ± 1.73	2.66 ± 9.35	0.02 ± 0.14	-0.01 ± 0.01	-0.06 ± 0.70	0.98 ± 0.70
	1-2	1.45 ± 0.50	0.48 ± 2.04	3.28 ± 9.17	0.04 ± 0.16	-0.01 ± 0.01	-0.11 ± 0.74	1.11 ± 1.24
	1-3	1.19 ± 0.52	0.58 ± 1.94	3.64 ± 9.56	0.08 ± 0.14	-0.00 ± 0.02	-0.04 ± 0.66	1.11 ± 1.17
	1-4	0.98 ± 0.57	1.25 ± 1.92	4.64 ± 10.26	0.08 ± 0.13	-0.00 ± 0.02	-0.02 ± 0.62	1.22 ± 1.08
G202	1	1.55 ± 0.53	0.10 ± 0.47	2.43 ± 10.43	0.06 ± 0.03	0.02 ± 0.01	0.03 ± 0.08	0.29 ± 0.14
	1-2	1.13 ± 0.58	0.19 ± 0.77	2.70 ± 9.61	0.05 ± 0.03	0.02 ± 0.02	0.03 ± 0.28	0.32 ± 0.34
	1-3	0.83 ± 0.58	0.27 ± 0.80	4.78 ± 8.82	0.04 ± 0.03	0.02 ± 0.02	0.03 ± 0.31	0.43 ± 0.39
	1-4	0.77 ± 0.57	0.28 ± 0.79	3.71 ± 8.63	0.04 ± 0.04	0.02 ± 0.03	0.04 ± 0.32	0.56 ± 0.44
G208 $N_{\mathcal{H}}$	1	11.81 ± 13.51	0.07 ± 0.07	3.72 ± 9.51	0.07 ± 0.12	0.03 ± 0.04	0.01 ± 0.02	0.11 ± 0.02
	1-2	7.48 ± 11.45	0.07 ± 0.12	3.45 ± 8.21	-0.00 ± 0.10	0.03 ± 0.06	0.00 ± 0.02	0.13 ± 0.05
	1-3	5.57 ± 10.26	0.07 ± 0.23	3.24 ± 8.17	-0.00 ± 0.09	0.03 ± 0.07	0.00 ± 0.03	0.13 ± 0.10
	1-4	3.71 ± 9.41	0.07 ± 0.31	3.13 ± 8.45	-0.00 ± 0.08	0.03 ± 0.07	-0.00 ± 0.04	0.15 ± 0.13
G208$N_{\mathcal{H},\rm crop}$	1	7.90 ± 1.42	0.16 ± 0.03	15.39 ± 5.17	1.08 ± 0.50	2.19 ± 2.59	-0.01 ± 0.01	0.10 ± 0.01
	1-2	5.13 ± 2.17	0.15 ± 0.03	15.58 ± 6.85	0.99 ± 0.57	1.96 ± 2.65	-0.01 ± 0.01	0.09 ± 0.01
	1-3	3.94 ± 2.26	0.14 ± 0.04	15.39 ± 7.76	0.63 ± 0.55	1.79 ± 2.42	-0.00 ± 0.02	0.08 ± 0.02
	1-4	3.43 ± 2.42	0.14 ± 0.04	11.95 ± 8.20	0.52 ± 0.55	1.42 ± 2.22	-0.00 ± 0.02	0.10 ± 0.03
G208 $N_{\mathcal{F}}$	1	12.90 ± 4.30	0.02 ± 0.02	2.72 ± 6.60	0.35 ± 0.89	4.62 ± 5.02	0.00 ± 0.01	0.04 ± 0.02
	1-2	9.03 ± 4.88	0.02 ± 0.04	2.74 ± 7.60	0.82 ± 0.88	2.85 ± 4.64	0.00 ± 0.01	0.05 ± 0.02
	1-3	6.64 ± 4.77	0.02 ± 0.04	2.58 ± 7.63	0.53 ± 0.83	2.47 ± 4.08	0.01 ± 0.02	0.06 ± 0.03
	1-4	5.32 ± 4.87	0.03 ± 0.04	2.50 ± 7.98	0.32 ± 0.79	2.16 ± 3.60	0.00 ± 0.02	0.07 ± 0.04

Notes. As in Table D.1 but for symmetric fits.

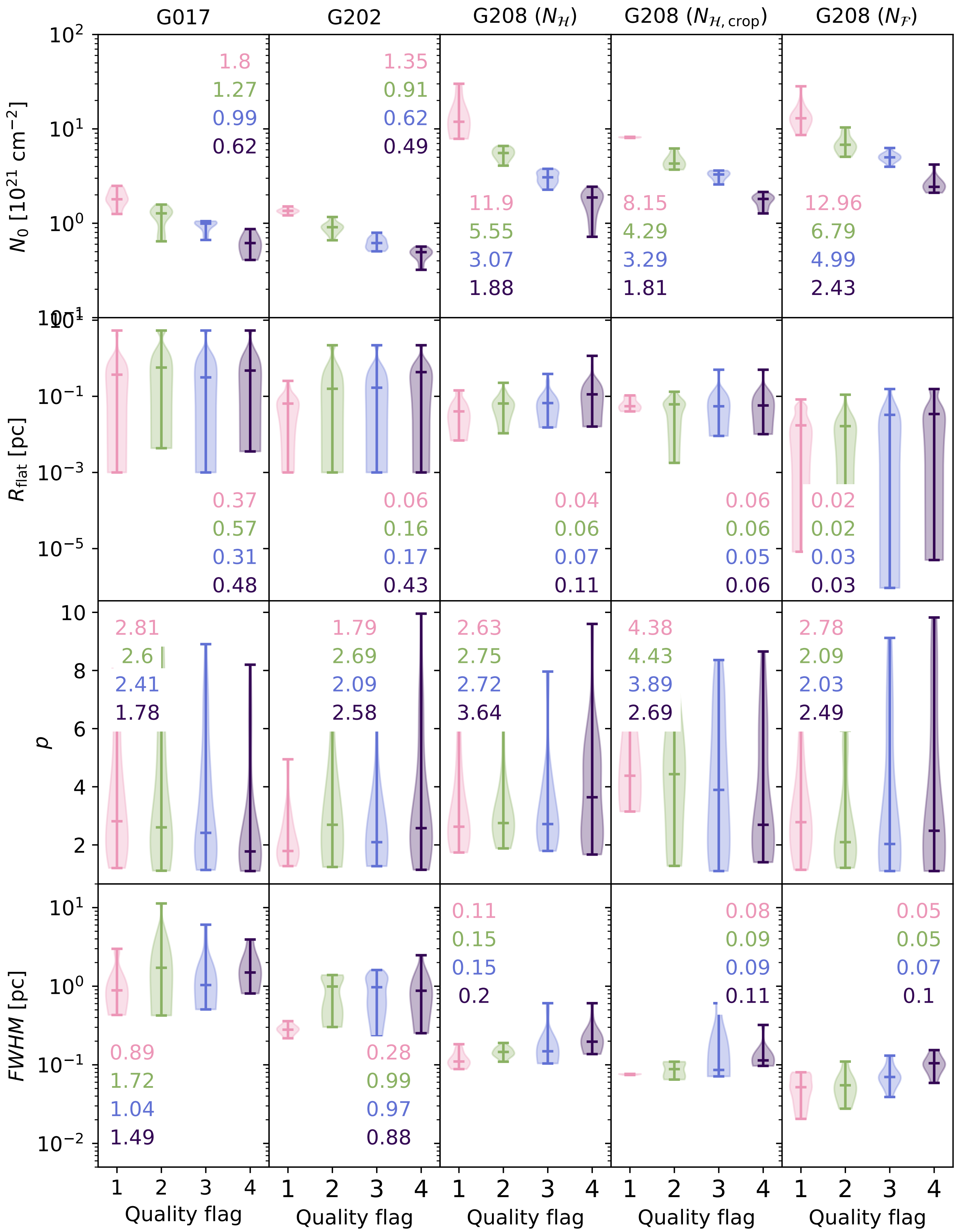

Fig. D.1. Violin plots of derived Plummer parameters for each quality bin for all fields used in this paper, for those fields with $p \leq 10$.